

Finite-Entanglement Scaling of 2D Metals

Quinten Mortier^{1,*}, Ming-Hao Li^{2,*}, Jutho Haegeman¹, and Nick Bultinck^{1,2}

¹*Department of Physics, Ghent University, Krijgslaan 281, 9000 Gent, Belgium*

²*Rudolf Peierls Centre for Theoretical Physics, University of Oxford, Parks Road, Oxford OX1 3PU, United Kingdom*

 (Received 17 May 2023; revised 27 September 2023; accepted 21 November 2023; published 27 December 2023)

We extend the study of finite-entanglement scaling from one-dimensional gapless models to two-dimensional systems with a Fermi surface. In particular, we show that the entanglement entropy of a contractible spatial region with linear size L scales as $S \sim L \log[\xi f(L/\xi)]$ in the optimal tensor network, and hence area-law entangled, state approximation to a metallic state, where $f(x)$ is a scaling function which depends on the shape of the Fermi surface and ξ is a finite correlation length induced by the restricted entanglement. Crucially, the scaling regime can be realized with numerically tractable bond dimensions. We also discuss the implications of the Lieb-Schultz-Mattis theorem at fractional filling for tensor network state approximations of metallic states.

DOI: 10.1103/PhysRevLett.131.266202

Introduction.—In the last two decades it has become increasingly clear that ground states of local lattice Hamiltonians have an interesting and rich entanglement structure. For example, generic ground states of *gapped* local Hamiltonians are observed to satisfy the so-called “area law” for the entanglement entropy of a subregion, meaning that the leading term in the entanglement entropy scales with the area of the boundary separating the subregion from the rest of the system (in 1D, the area law has been proven; see Ref. [1]). Furthermore, subleading corrections to the area law contain universal information about the topological phase of the system [2,3]. Related quantities, such as the entanglement spectrum [4] and multipartite entanglement measures [5–11], have also been shown to reveal topological information.

In the case of gapless local Hamiltonians, the area law is frequently violated. Two notable examples are gapless 1D systems with long-wavelength properties that can be described by conformal field theory (CFT), and systems in higher dimensions with a Fermi surface. In the former case, the entanglement of a subregion with linear size L scales as $S \sim c/3 \log L$, with c the central charge of the CFT [12–14], whereas $S \sim L^{d-1} \log L$ in a d -dimensional system exhibiting a codimension 1 Fermi surface [15–18].

The entanglement structure of ground states has direct practical consequences for classical simulations of quantum systems. The existence of an area law is both a necessary condition as well as a strong motivation to represent the ground state as a tensor network state (TNS) [19–22]. TNSs are compressed representations of quantum states in terms of local tensors which can be stored and manipulated efficiently by classical computers, and therefore present a useful variational space for numerical studies. For systems violating the area law, the theory of “finite-entanglement scaling” [23–28] describes how an area-law state (i.e., a TNS) best approximates the non-area-law ground state in the

thermodynamic limit. A remarkable result from finite-entanglement scaling is that for 1D critical ground states described by a CFT, the restricted entanglement induced by the finite TNS bond dimension D (i.e., the dimension of the contracted indices of the tensors) results in a finite correlation length $\xi \propto D^\kappa$, where κ is a universal number determined by the central charge of the CFT [23,24]. As a result, the entanglement entropy of a region of length L can be expressed in terms of a scaling function which depends only on the ratio L/D^κ [23,24,29].

In this Letter we extend the finite-entanglement scaling analysis to two dimensions and show that a similar scaling collapse is possible for the entanglement entropy of metals, i.e., states with a Fermi surface, despite the fact that there is no underlying CFT describing the long-wavelength physics. Our results show that by exploiting the scaling collapse, moderate (and numerically tractable) bond dimensions already give rise to a sufficiently high numerical accuracy to reliably access all information about the Fermi surface that is contained in the Widom formula, and hence apply the general approach of “entanglement spectroscopy” to metallic systems. Some interesting previous works have studied finite-correlation-length scaling for 2D TNS [30–33], but these works did not consider area-law-violating ground states.

Gaussian fermionic TNS.—For concreteness we will perform our analysis on a square lattice. Since we are interested in 2D states with a Fermi surface we use fermionic projected entangled-pair states (PEPS) [34–39]. In particular, we will be working with *Gaussian* fermionic tensors, which produce either a Slater determinant or a Bardeen-Cooper-Schrieffer (BCS) pairing (or pfaffian) state after contraction of the virtual indices. To define the Gaussian tensors, we assign fermion creation operators $f_{\mathbf{x},a}^\dagger$ ($a \in \{1, \dots, N\}$) to the physical index of the tensor at site \mathbf{x} , and

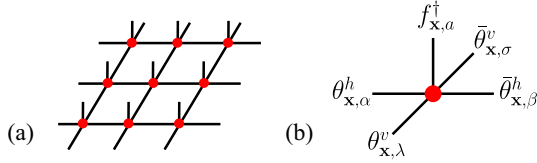


FIG. 1. (a) A 2D tensor network on a 3×3 square lattice. (b) The assignment of physical creation operators $f_{\mathbf{x}}^\dagger$ to the physical index, and virtual Grassmann variables $\theta_{\mathbf{x}}, \bar{\theta}_{\mathbf{x}}$ to the virtual indices, of a Gaussian fermionic tensor.

Grassmann variables $\theta_{x,\alpha}^h, \bar{\theta}_{x,\beta}^h, \theta_{x,\lambda}^v, \bar{\theta}_{x,\sigma}^v$ ($\alpha, \beta, \lambda, \sigma \in \{1, \dots, M\}$) to the virtual indices, as in Fig. 1. The Grassmann variables square to zero, are mutually anticommuting, and also anticommute with the creation operators $f_{x,a}^\dagger$. The Gaussian tensor at site \mathbf{x} is defined as

$$\hat{T}_{\mathbf{x}} = \exp\left(\frac{1}{2}\chi_{\mathbf{x}}^T A \chi_{\mathbf{x}}\right), \quad (1)$$

where the column vector $\chi_{\mathbf{x}} \equiv (f_{\mathbf{x}}^\dagger, \theta_{\mathbf{x}}^h, \bar{\theta}_{\mathbf{x}}^h, \theta_{\mathbf{x}}^v, \bar{\theta}_{\mathbf{x}}^v)$ collects the N creation operators and $4M$ Grassmann variables assigned to site \mathbf{x} , and the antisymmetric matrix $A \in \mathbb{C}^{(N+4M) \times (N+4M)}$ contains the variational parameters. Note that A is independent of \mathbf{x} , which means that we are restricting ourselves to translation-invariant (TI) states. With the definition of the tensors in place, we can now define the (unnormalized) contracted Gaussian fermionic TNS (GfTNS) via the Berezin integral [40]

$$|\psi\rangle = \int [D\theta] \int [D\bar{\theta}] \prod_{\mathbf{x}} e^{\bar{\theta}_{\mathbf{x}}^T \theta_{\mathbf{x}+\mathbf{e}_x}^h} e^{\bar{\theta}_{\mathbf{x}}^T \theta_{\mathbf{x}+\mathbf{e}_y}^v} \hat{T}_{\mathbf{x}} |0\rangle, \quad (2)$$

where $|0\rangle$ is the physical Fock vacuum and $\mathbf{e}_{x/y}$ are unit vectors along the x/y direction. Every Grassmann variable spans a two-dimensional super vector space, so the bond dimension of the GfTNS is $D = 2^M$.

Because we are considering TI states, the Gaussian Grassmann integral in Eq. (2) can be further simplified by going to momentum space. Working with a large but finite system of $N_s = N_x N_y$ sites and (anti-)periodic boundary conditions while defining $\chi_{\mathbf{k}} = (1/\sqrt{N_s}) \sum_{\mathbf{x}} e^{i\mathbf{k}\cdot\mathbf{x}} \chi_{\mathbf{x}}$, we can write

$$|\psi\rangle = \int [D\theta] \int [D\bar{\theta}] \exp\left(\frac{1}{2} \sum_{\mathbf{k}} \chi_{-\mathbf{k}}^T [A + M(\mathbf{k})] \chi_{\mathbf{k}}\right) |0\rangle.$$

Here, $M(\mathbf{k})$ is defined as $M(\mathbf{k}) = \mathbf{0}_N \oplus \tilde{M}(\mathbf{k})$, with $\mathbf{0}_N$ a $N \times N$ zero matrix, and

$$\tilde{M}(\mathbf{k}) = \begin{pmatrix} \mathbf{0}_M & -e^{ik_x} \mathbb{1}_M \\ e^{-ik_x} \mathbb{1}_M & \mathbf{0}_M \end{pmatrix} \oplus \begin{pmatrix} \mathbf{0}_M & -e^{ik_y} \mathbb{1}_M \\ e^{-ik_y} \mathbb{1}_M & \mathbf{0}_M \end{pmatrix}. \quad (3)$$

Writing $A = \begin{pmatrix} B & -C^T \\ C & D \end{pmatrix}$, with $N \times N$ submatrix B , $4M \times N$ submatrix C , and $4M \times 4M$ submatrix D , we finally obtain

$$|\psi\rangle \propto e^{\frac{1}{2} \sum_{\mathbf{k}} f_{-\mathbf{k}}^\dagger \{B + C^T [D + \tilde{M}(\mathbf{k})]^{-1} C\} f_{\mathbf{k}}^\dagger} |0\rangle. \quad (4)$$

Here, we have assumed that $D + \tilde{M}(\mathbf{k})$ is nondegenerate at every \mathbf{k} and refer to Ref. [41] for the degenerate case.

The construction of GfTNS as presented here was introduced in Ref. [37], and has been used in previous studies [38,42,62,63]. There also exists an alternative formulation in terms of density matrices [34]. For our results presented below we have used both formalisms, each of which has different practical advantages. However, the two formalisms are ultimately equivalent and can be translated into each other [41].

The state in Eq. (4) takes the form of a general BCS pairing state. Given that we set out to study states with a Fermi surface, the reader might worry that we are using TNS which contract to pairing states. The reason for this is simply that a finite- D Gaussian fTNS with explicit charge conservation symmetry always has an integer particle number at every momentum which is constant throughout the Brillouin zone, and therefore cannot represent or even closely approximate a state with a Fermi surface. This is not an embarrassing shortcoming of GfTNS, but a direct consequence of the Lieb-Schultz-Mattis theorem, which states that one cannot have a trivial insulator at noninteger fillings [64–67]. In particular, in Ref. [68], it was shown that if a general, explicitly TI and $U(1)$ -symmetric fTNS is forced to have a filling $\nu = p/q$, with p and $q > 1$ coprime integers, then the tensors necessarily have a purely virtual \mathbb{Z}_{2q} symmetry. The entanglement entropy (EE) in a generic tensor network state with such virtual symmetry scales as $S = \alpha L - \ln 2q + \mathcal{O}(L^{-1})$, which implies that the fTNS has nontrivial topological order [43,69–71]. So the incompatibility of Gaussianity and explicit $U(1)$ symmetry at fractional filling $\nu = p/q$ for fTNS is a manifestation of the simple fact that Slater determinants cannot represent states with nontrivial topological order. The only way for a TI GfTNS to introduce finite entanglement in a metallic state is therefore to open a small superconducting gap at the Fermi surface.

Spinless fermions.—We first consider the case with $N = 1$, i.e., spinless fermions with a single orbital per site. To obtain the GfTNS, we minimize the energy of the following simple hopping Hamiltonian:

$$H = -t \sum_{\langle ij \rangle} f_i^\dagger f_j - t' \sum_{\langle\langle ij \rangle\rangle} f_i^\dagger f_j + \text{H.c.} - \mu \sum_i f_i^\dagger f_i, \quad (5)$$

where the first (second) sum is over nearest (next-nearest) neighbors. We choose the chemical potential μ such that there is a single electron pocket centered at the Γ point. With periodic boundary conditions, the total number of electrons in the spinless Fermi sea is odd for every system

size. If a state at momentum \mathbf{k} is occupied, then so is the state at $-\mathbf{k}$. So the electrons appear in pairs, except at the time-reversal invariant momenta (TRIM). Here, the only TRIM which is occupied is the center of Brillouin zone $\mathbf{k} = 0$; hence the overall fermion parity is odd. The tensors defined in Eq. (1) have even fermion parity, and therefore the GfTNS also necessarily has even parity (for every system size). This is reflected in the fact that the wave function in Eq. (4) with $N = 1$ always leaves the states at the TRIM empty. It is possible to fix this discrepancy by inserting an additional Grassmann variable “on the virtual level” in Eq. (2), which makes the fTNS have odd parity [41] (this Grassmann variable is identical to the string operators that have appeared in fTNS constructions [44] of the $p_x + ip_y$ superconductor [45]). Here, however, we will use a simpler way to sidestep this issue and work with antiperiodic boundary conditions such that the spinless Fermi surface state always has even fermion parity.

We choose μ to fix the total particle number N_e at half filling, i.e., $\nu = N_e/N_s = 1/2$, and use $t'/t = 0.353$ to realize an almost circular Fermi surface. We have optimized the GfTNS to minimize its energy $\langle H \rangle$, at different bond dimensions D (see Ref. [41] for details of the numerical simulations). Figure 2(a) depicts the difference in energy of the optimal GfTNS compared with the exact result, as well as the standard deviation of the total particle number per site, i.e., $\sigma_q \equiv \sqrt{\langle N_e^2 \rangle - \langle N_e \rangle^2} / N_s$. The latter is a quantifier for the charge conservation symmetry breaking in the GfTNS. We see that both the energy error and σ_q decrease as a function of D , indicating—similarly to Ref. [46]—that the optimized GfTNS provides an approximation to the exact metallic ground state which improves systematically with bond dimension. Figure 2(b) shows the correlation function $G(\mathbf{r}) = \langle f_{\mathbf{r}+\mathbf{r}'}^\dagger f_{\mathbf{r}'} \rangle$ of the $D = 16$ GfTNS, which agrees with the exact result for $|\mathbf{r}| \lesssim \xi \approx 70$. Note that $\xi \ll N_x = N_y$, such that we can take our results to be representative of the thermodynamic limit. In Figs. 2(c) and 2(d) we plot the pairing function $\langle f_{\mathbf{k}} f_{-\mathbf{k}} \rangle$ for $D = 32$, both along a radial cut, and throughout the entire Brillouin zone. $|\langle f_{\mathbf{k}} f_{-\mathbf{k}} \rangle|^2$ is peaked at the Fermi surface, and can be approximated by the BCS expression $\Delta^2 / 4(\Delta^2 + \varepsilon_{\mathbf{k}}^2)$, where $\varepsilon_{\mathbf{k}}$ is the single-particle dispersion of H . Figure 2(d) illustrates that the phase of $\langle f_{\mathbf{k}} f_{-\mathbf{k}} \rangle$ winds by 2π along the Fermi surface, i.e., it is a $p_x + ip_y$ gap. We explain how the GfTNS deals with the chiral topology of the weak-pairing $p_x + ip_y$ superconductor [42,45,47] in the Supplemental Material [41].

The leading term in the EE of a square $L \times L$ spatial region R in a 2D state with a single spinless Fermi surface is given by

$$S = \frac{\log(\Lambda L)}{24\pi} \oint_{\partial R} \oint_{FS} |dS_{\mathbf{x}} \cdot dS_{\mathbf{k}}|, \quad (6)$$

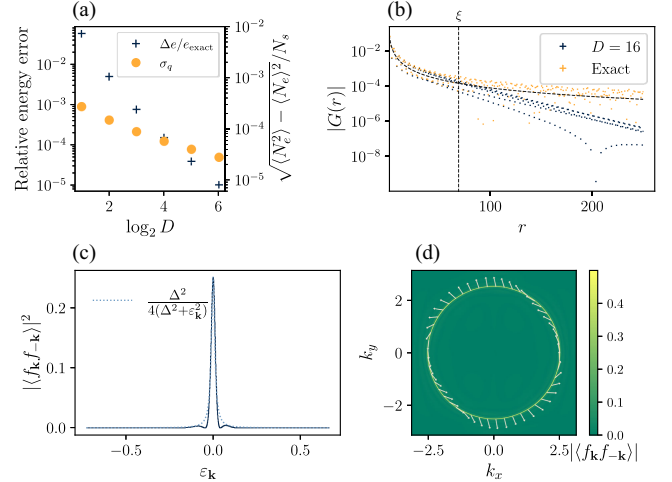


FIG. 2. Results for spinless fermions with $t'/t = 0.353$ at half filling of $N_s = 999^2$ sites. (a) Relative difference in energy per site (denoted as $\Delta e/e_{\text{exact}}$) between the exact ground state and the optimized GfTNS as a function of bond dimension D ; and the standard deviation σ_q of the particle number per site of the optimized GfTNS. (b) $|\langle f_{\mathbf{r}} f_{\mathbf{0}} \rangle|$ for $D = 16$ GfTNS vs the exact ground state. Near ξ , which is extracted from the EE, $|G(r)|$ for GfTNS starts to decay much faster than the power law behavior for that of the exact ground state. (c) $|\langle f_{\mathbf{k}} f_{-\mathbf{k}} \rangle|^2$ at $D = 32$ along a radial direction in the Brillouin zone as a function of the single-particle energy $\varepsilon_{\mathbf{k}}$ of H [Eq. (5)]. (d) $\langle f_{\mathbf{k}} f_{-\mathbf{k}} \rangle$ at $D = 32$ throughout the Brillouin zone. The color map denotes the magnitude, the arrows the complex phase.

where Λ is a nonuniversal inverse length scale, and the integrals are over the boundary of R and over the Fermi surface, and $dS_{\mathbf{x}}$ ($dS_{\mathbf{k}}$) is a surface element of ∂R (the Fermi surface) [16]. For the special case of a circular Fermi surface with radius k_F , this general expression evaluates to $S_{\text{circ}} = (2k_F L / 3\pi) \log \Lambda L$.

In Fig. 3(a), we plot the EE S as a function of L , directly calculated from the correlation matrix of the optimized GfTNS at different D . This plot shows our main result, which is that the leading contribution to the EE at finite D can be written as

$$S_{\text{fTNS}} = \log(\Lambda \xi f(L/\xi)) \times \frac{1}{24\pi} \oint_{\partial R} \oint_{FS} |dS_{\mathbf{x}} \cdot dS_{\mathbf{k}}|, \quad (7)$$

where ξ is the finite-bond-dimension-induced correlation length, and $f(x)$ is a scaling function which satisfies $f(x \ll 1) \sim x$ and $f(x \gg 1) = \text{constant}$. Figure 3(a) shows how the optimized GfTNS at different D approximate the $L \log L$ scaling of the EE, while Fig. 3(b) directly plots the scaling function $f(x)$ onto which the numerical data obtained at different D can be collapsed. Note that to obtain the scaling collapse we have only one tuning parameter ξ if we require that the GfTNS results agree with the exact result at small L . The length scale ξ obtained from the EE of the $D = 16$ GfTNS [41] is indicated as the

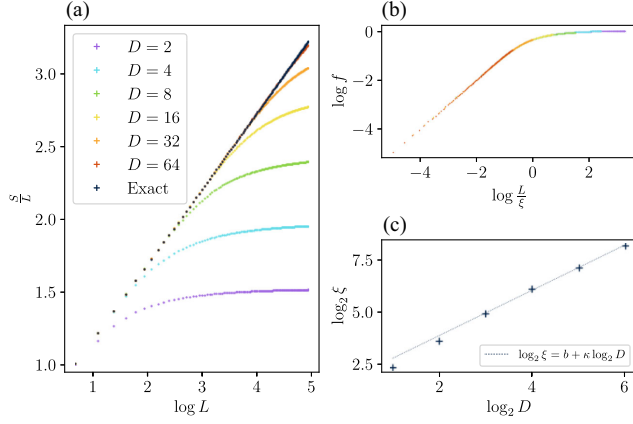


FIG. 3. (a) Scaling collapse of the entanglement entropy S of a $L \times L$ square region in the optimised GfTNS for spinless fermions at half filling with $t'/t = 0.353$ and $N_s = 999^2$, obtained at different bond dimensions D . (b) Collapse of the GfTNS entanglement entropies using the scaling law of Eq. (7). (c) Linear fit of the correlation length ξ as a function of D obtained from the scaling collapse of S , with $\kappa = 1.074$.

vertical dashed line in the plot of $G(\mathbf{r})$ in Fig. 2(b). This shows that ξ agrees with the physical correlation length, i.e., the length scale at which the exponential decay of correlations in the GfTNS sets in. Finally, Fig. 3(c) confirms that ξ increases monotonically as a function of D . For the moderate bond dimensions used in this Letter, ξ seems to follow a power law as a function of D . However, based on both analytical [48] and numerical [41] results in 1D, which show that Gaussian fermionic matrix product states (GfMPS) cannot reproduce the power-law scaling $\xi \propto D^\kappa$ of generic matrix product states, we anticipate that for GfTNS, deviations from the power-law relation between ξ and D could occur at higher D . For general (i.e., non-Gaussian) fTNS, we nevertheless conjecture that $\xi \propto D^\kappa$.

Spinful fermions.—Next, we consider the same Hamiltonian as in Eq. (5), but now for spinful fermions ($N = 2$) created by $f_{\mathbf{x},\sigma}^\dagger$ with $\sigma = \uparrow, \downarrow$. An important difference between the spinless and spinful models lies in the nature of the superconducting gap of the optimal GfTNS approximation. In particular, as we explicitly impose SU(2) spin symmetry on the GfTNS, the superconducting gap will be spin singlet and hence even under inversion.

We now verify whether the finite-entanglement scaling law (7) also holds for the spinful model. In doing so, we have used the density-matrix-based method for GfTNS [34,41], and a numerical optimization which relies on minimizing the Frobenius norm of the difference between the exact single-particle density matrix and the GfTNS density matrix (see Ref. [41] for details). Note that the virtual fermion degrees of freedom now carry spin-1/2, which means that the bond dimension D is restricted to occur in powers of 4.

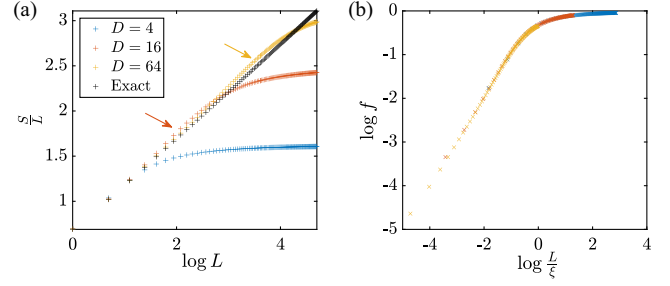


FIG. 4. (a) Entanglement entropies for a $L \times L$ square subsystem in the exact ground state and its GfTNS approximations with the indicated bond dimensions. Up to a bulk correlation length ξ the exact profile is reproduced. After the transition region with a characteristic ‘‘bump’’ (marked by the arrows), the GfTNS profiles saturate. (b) Collapse of the GfTNS entanglement entropies using the scaling law of Eq. (7).

As for the spinless model, we have computed the EE of a $L \times L$ region R for the spinful Fermi surface model and its GfTNS approximations. The spinful results displayed in Fig. 4 show a similar behavior to the spinless results in Fig. 3, with some minor differences. In particular, right before the EE reaches the area-law regime (signaled by the plateau in Fig. 4), we discern a small ‘‘bump’’ where S_{fTNS} rises slightly above the exact value for S (indicated by the arrows in Fig. 4). We attribute this to the correlations between the different spin flavors induced by the singlet pairing. Another difference is the generally lower ξ values for the same bond dimension. This is a consequence of the increased local Hilbert space dimension. Also, the rate at which ξ increases with D is lower than in the spinless case, which is reminiscent of the 1D case, where an increase in the central charge lowers the exponent κ in $\xi \propto D^\kappa$. Besides these minor differences, Fig. 4(b) confirms our main result, which is that the EE at different D can be collapsed using the scaling law in Eq. (7).

Properties of the scaling function.—Similarly to the scaling functions of gapless systems with conformal symmetry in the IR, $f(x)$ is expected to be insensitive to lattice-scale details. We also expect that $f(x)$ will depend on the shape of the Fermi surface, in analogy to the finite-temperature entropy scaling functions for Fermi liquids [49]. To verify the first expectation we have performed numerical data collapses of the EE obtained at different fillings, while keeping the Fermi surface (FS) approximately circular. These results [41] confirm that the EE at different fillings can indeed be collapsed on the same curve. By tuning away from $t'/t = 0.353$ in either direction, which changes the FS to being either more diamondlike or more squarelike, we observe that the results collapse on different scaling functions, thus confirming the dependence of $f(x)$ on the FS geometry [41].

Conclusions.—We have shown that the theory of finite-entanglement scaling can be generalized from 1D gapless systems to 2D states with a Fermi surface. Our main result is

that $S_{\text{FTNS}}(L, D)$, the EE of a $L \times L$ spatial region in the optimal bond-dimension- D fTNS approximation of a metallic state, can be written as $S_{\text{FTNS}}(L, D) \sim L \log(\xi_D f(L/\xi_D))$, where ξ_D is a finite infrared length scale which results from the area-law structure (and thus the finite bond dimension D) of the tensor network state, and $f(x)$ is a scaling function which depends on the shape of the Fermi surface, but not on the length scale k_F^{-1} , with k_F the Fermi momentum.

Fermionic tensor networks are being used in a variety of different ways, e.g., for numerical studies of lattice gauge theories [72–74], as numerically tractable Gutzwiller-projected states [75–81], as a tool for large-scale mean-field calculations [50,82], as trial states for topological phases [42,43,47,51,83–85], and as a general class of variational states for numerical simulations of strongly interacting systems [36,86–90]. The results presented in this Letter show how these applications of fTNS can be extended to metallic states. In particular, being able to perform a scaling collapse for the EE provides solid numerical evidence for the existence of a Fermi surface, and hence can be used to numerically determine whether the ground state of Hubbard-type models (e.g., those obtained from the flat bands of twisted transition-metal dichalcogenides) are metallic or insulating. Similarly, a scaling collapse for the EE can be used to determine whether a frustrated spin model has a spin liquid ground state with a spinon Fermi surface. Furthermore, the scaling collapse significantly enhances the accuracy of the numerically obtained Widom prefactor, and hence provides more reliable information about the fermiology of the metallic ground states.

We acknowledge useful discussions with Hong-Hao Tu, Mike Zaletel, Roger Mong, Ignacio Cirac, Siddharth Parameswaran, and Steven R. White. We also thank Siddharth Parameswaran for helpful feedback on an earlier version of the manuscript. Q. M. and J. H. have received support from the European Research Council (ERC) under the European Union’s Horizon 2020 program [Grant Agreement No. 715861 (ERQUAF)] and from the Research Foundation Flanders. N. B. was supported by a University Research Fellowship of the Royal Society. M. L. has received support from the European Research Council under the European Union Horizon 2020 Research and Innovation Programme, through Starting Grant [Agreement No. 804213-TMCS], and from a Buckee Scholarship at Merton College.

*These authors contributed equally to this work.

- [1] M. B. Hastings, An area law for one-dimensional quantum systems, *J. Stat. Mech.* (2007) P08024.
- [2] A. Kitaev and J. Preskill, Topological entanglement entropy, *Phys. Rev. Lett.* **96**, 110404 (2006).
- [3] M. Levin and X.-G. Wen, Detecting topological order in a ground state wave function, *Phys. Rev. Lett.* **96**, 110405 (2006).
- [4] H. Li and F. D. M. Haldane, Entanglement spectrum as a generalization of entanglement entropy: Identification of topological order in non-Abelian fractional quantum Hall effect states, *Phys. Rev. Lett.* **101**, 010504 (2008).
- [5] Y. Zou, K. Siva, T. Soejima, R. S. K. Mong, and M. P. Zaletel, Universal tripartite entanglement in one-dimensional many-body systems, *Phys. Rev. Lett.* **126**, 120501 (2021).
- [6] K. Siva, Y. Zou, T. Soejima, R. S. K. Mong, and M. P. Zaletel, Universal tripartite entanglement signature of un-gappable edge states, *Phys. Rev. B* **106**, L041107 (2022).
- [7] Y. Liu, R. Sohal, J. Kudler-Flam, and S. Ryu, Multipartitioning topological phases by vertex states and quantum entanglement, *Phys. Rev. B* **105**, 115107 (2022).
- [8] Y. Liu, Y. Kusuki, J. Kudler-Flam, R. Sohal, and S. Ryu, Multipartite entanglement in two-dimensional chiral topological liquids, [arXiv:2301.07130](https://arxiv.org/abs/2301.07130).
- [9] I. H. Kim, B. Shi, K. Kato, and V. V. Albert, Chiral central charge from a single bulk wave function, *Phys. Rev. Lett.* **128**, 176402 (2022).
- [10] P. M. Tam, M. Claassen, and C. L. Kane, Topological multipartite entanglement in a Fermi liquid, *Phys. Rev. X* **12**, 031022 (2022).
- [11] R. Sohal and S. Ryu, Entanglement in tripartitions of topological orders: A diagrammatic approach, *Phys. Rev. B* **108**, 045104 (2023).
- [12] C. Holzhey, F. Larsen, and F. Wilczek, Geometric and renormalized entropy in conformal field theory, *Nucl. Phys. B* **424**, 443 (1994).
- [13] G. Vidal, J. I. Latorre, E. Rico, and A. Kitaev, Entanglement in quantum critical phenomena, *Phys. Rev. Lett.* **90**, 227902 (2003).
- [14] P. Calabrese and J. Cardy, Entanglement entropy and quantum field theory, *J. Stat. Mech.* (2004) P06002.
- [15] M. M. Wolf, Violation of the entropic area law for fermions, *Phys. Rev. Lett.* **96**, 010404 (2006).
- [16] D. Gioev and I. Klich, Entanglement entropy of fermions in any dimension and the Widom conjecture, *Phys. Rev. Lett.* **96**, 100503 (2006).
- [17] B. Swingle, Entanglement entropy and the Fermi surface, *Phys. Rev. Lett.* **105**, 050502 (2010).
- [18] W. Ding, A. Seidel, and K. Yang, Entanglement entropy of Fermi liquids via multidimensional bosonization, *Phys. Rev. X* **2**, 011012 (2012).
- [19] M. Fannes, B. Nachtergaele, and R. F. Werner, Finitely correlated states on quantum spin chains, *Commun. Math. Phys.* **144**, 443 (1992).
- [20] F. Verstraete and J. I. Cirac, Valence-bond states for quantum computation, *Phys. Rev. A* **70**, 060302(R) (2004).
- [21] F. Verstraete and J. I. Cirac, Renormalization algorithms for quantum-many body systems in two and higher dimensions, [arXiv:cond-mat/0407066](https://arxiv.org/abs/cond-mat/0407066).
- [22] J. I. Cirac, D. Pérez-García, N. Schuch, and F. Verstraete, Matrix product states and projected entangled pair states: Concepts, symmetries, theorems, *Rev. Mod. Phys.* **93**, 045003 (2021).
- [23] L. Tagliacozzo, T. R. de Oliveira, S. Iblisdir, and J. I. Latorre, Scaling of entanglement support for matrix product states, *Phys. Rev. B* **78**, 024410 (2008).

- [24] F. Pollmann, S. Mukerjee, A. M. Turner, and J. E. Moore, Theory of finite-entanglement scaling at one-dimensional quantum critical points, *Phys. Rev. Lett.* **102**, 255701 (2009).
- [25] B. Pirvu, G. Vidal, F. Verstraete, and L. Tagliacozzo, Matrix product states for critical spin chains: Finite-size versus finite-entanglement scaling, *Phys. Rev. B* **86**, 075117 (2012).
- [26] V. Stojevic, J. Haegeman, I. P. McCulloch, L. Tagliacozzo, and F. Verstraete, Conformal data from finite entanglement scaling, *Phys. Rev. B* **91**, 035120 (2015).
- [27] N. E. Sherman, A. Avdoshkin, and J. E. Moore, Universality of critical dynamics with finite entanglement, *Phys. Rev. Lett.* **131**, 106501 (2023).
- [28] A. Ueda and M. Oshikawa, Finite-size and finite bond dimension effects of tensor network renormalization, *Phys. Rev. B* **108**, 024413 (2023).
- [29] P. Calabrese and J. Cardy, Entanglement entropy and conformal field theory, *J. Phys. A* **42**, 504005 (2009).
- [30] P. Corboz, P. Czarnik, G. Kapteijns, and L. Tagliacozzo, Finite correlation length scaling with infinite projected entangled-pair states, *Phys. Rev. X* **8**, 031031 (2018).
- [31] M. Rader and A. M. Läuchli, Finite correlation length scaling in Lorentz-invariant gapless IPEPS wave functions, *Phys. Rev. X* **8**, 031030 (2018).
- [32] P. Czarnik and P. Corboz, Finite correlation length scaling with infinite projected entangled pair states at finite temperature, *Phys. Rev. B* **99**, 245107 (2019).
- [33] B. Vanhecke, J. Hasik, F. Verstraete, and L. Vanderstraeten, Scaling hypothesis for projected entangled-pair states, *Phys. Rev. Lett.* **129**, 200601 (2022).
- [34] C. V. Kraus, N. Schuch, F. Verstraete, and J. I. Cirac, Fermionic projected entangled pair states, *Phys. Rev. A* **81**, 052338 (2010).
- [35] T. Barthel, C. Pineda, and J. Eisert, Contraction of fermionic operator circuits and the simulation of strongly correlated fermions, *Phys. Rev. A* **80**, 042333 (2009).
- [36] P. Corboz, R. Orús, B. Bauer, and G. Vidal, Simulation of strongly correlated fermions in two spatial dimensions with fermionic projected entangled-pair states, *Phys. Rev. B* **81**, 165104 (2010).
- [37] Z.-C. Gu, F. Verstraete, and X.-G. Wen, Grassmann tensor network states and its renormalization for strongly correlated fermionic and bosonic states, [arXiv:1004.2563](https://arxiv.org/abs/1004.2563).
- [38] Z.-C. Gu, Efficient simulation of Grassmann tensor product states, *Phys. Rev. B* **88**, 115139 (2013).
- [39] N. Bultinck, D. J. Williamson, J. Haegeman, and F. Verstraete, Fermionic projected entangled-pair states and topological phases, *J. Phys. A* **51**, 025202 (2017).
- [40] F. Berezin, *The Method of Second Quantization*, Pure and Applied Physics: A Series of Monographs and Textbooks Vol. 24 (Academic Press, New York, 1966), <https://books.google.co.uk/books?id=fAIRAAAAMAAJ>.
- [41] See Supplemental Material at <http://link.aps.org/supplemental/10.1103/PhysRevLett.131.266202>, which includes Refs. [23–25, 34, 37, 42–61] for more information on the utilized Ansätze and their intricacies, on how to perform the scaling collapse and for additional results.
- [42] J. Dubail and N. Read, Tensor network trial states for chiral topological phases in two dimensions and a no-go theorem in any dimension, *Phys. Rev. B* **92**, 205307 (2015).
- [43] N. Bultinck, M. Mariën, D. Williamson, M. Şahinoğlu, J. Haegeman, and F. Verstraete, Anyons and matrix product operator algebras, *Ann. Phys. (Amsterdam)* **378**, 183 (2017).
- [44] T. B. Wahl, S. T. Haßler, H.-H. Tu, J. I. Cirac, and N. Schuch, Symmetries and boundary theories for chiral projected entangled pair states, *Phys. Rev. B* **90**, 115133 (2014).
- [45] N. Read and D. Green, Paired states of fermions in two dimensions with breaking of parity and time-reversal symmetries and the fractional quantum Hall effect, *Phys. Rev. B* **61**, 10267 (2000).
- [46] Q. Mortier, N. Schuch, F. Verstraete, and J. Haegeman, Tensor networks can resolve Fermi surfaces, *Phys. Rev. Lett.* **129**, 206401 (2022).
- [47] T. B. Wahl, H.-H. Tu, N. Schuch, and J. I. Cirac, Projected entangled-pair states can describe chiral topological states, *Phys. Rev. Lett.* **111**, 236805 (2013).
- [48] A. Franco-Rubio and J. I. Cirac, Gaussian matrix product states cannot efficiently describe critical systems, *Phys. Rev. B* **106**, 235136 (2022).
- [49] B. Swingle and T. Senthil, Universal crossovers between entanglement entropy and thermal entropy, *Phys. Rev. B* **87**, 045123 (2013).
- [50] N. Schuch and B. Bauer, Matrix product state algorithms for Gaussian fermionic states, *Phys. Rev. B* **100**, 245121 (2019).
- [51] N. Bultinck, D. J. Williamson, J. Haegeman, and F. Verstraete, Fermionic matrix product states and one-dimensional topological phases, *Phys. Rev. B* **95**, 075108 (2017).
- [52] A. Y. Kitaev, Unpaired Majorana fermions in quantum wires, *Phys. Usp.* **44**, 131 (2001).
- [53] H. Becker, On the transformation of a complex skew-symmetric matrix into a real normal form and its application to a direct proof of the Bloch-Messiah theorem, *Lettere al Nuovo Cimento* (1971–1985) **8**, 185 (1973).
- [54] P. K. Mogensén *et al.*, [JulianSolvers/optim.jl](https://pypi.org/project/JulianSolvers/): v1.7.4 (2022).
- [55] B. Vanhecke, J. Haegeman, K. Van Acoleyen, L. Vanderstraeten, and F. Verstraete, Scaling hypothesis for matrix product states, *Phys. Rev. Lett.* **123**, 250604 (2019).
- [56] N. Schuch, M. M. Wolf, and J. I. Cirac, Gaussian matrix product states, [arXiv:1201.3945](https://arxiv.org/abs/1201.3945).
- [57] S. Bravyi, Lagrangian representation for fermionic linear optics, *Quantum Inf. Comput.* **5**, 216 (2005).
- [58] N. Boumal, B. Mishra, P.-A. Absil, and R. Sepulchre, Manopt, a Matlab toolbox for optimization on manifolds, *J. Mach. Learn. Res.* **15**, 1455 (2014).
- [59] C.-K. Chiu, J. C. Y. Teo, A. P. Schnyder, and S. Ryu, Classification of topological quantum matter with symmetries, *Rev. Mod. Phys.* **88**, 035005 (2016).
- [60] J. Hasik, M. Van Damme, D. Poilblanc, and L. Vanderstraeten, Simulating chiral spin liquids with projected entangled-pair states, *Phys. Rev. Lett.* **129**, 177201 (2022).
- [61] A. Perelomov, *Generalized Coherent States and their Applications* (Springer-Verlag, Berlin, 1986).

- [62] B. Béri and N. R. Cooper, Local tensor network for strongly correlated projective states, *Phys. Rev. Lett.* **106**, 156401 (2011).
- [63] S. Yin, N. R. Cooper, and B. Béri, Strictly local tensor networks for short-range topological insulators, *Phys. Rev. B* **99**, 195125 (2019).
- [64] E. Lieb, T. Schultz, and D. Mattis, Two soluble models of an antiferromagnetic chain, *Ann. Phys. (N.Y.)* **16**, 407 (1961).
- [65] I. Affleck, Spin gap and symmetry breaking in CuO_2 layers and other antiferromagnets, *Phys. Rev. B* **37**, 5186 (1988).
- [66] M. Oshikawa, Commensurability, excitation gap, and topology in quantum many-particle systems on a periodic lattice, *Phys. Rev. Lett.* **84**, 1535 (2000).
- [67] M. B. Hastings, Lieb-Schultz-Mattis in higher dimensions, *Phys. Rev. B* **69**, 104431 (2004).
- [68] N. Bultinck and M. Cheng, Filling constraints on fermionic topological order in zero magnetic field, *Phys. Rev. B* **98**, 161119(R) (2018).
- [69] N. Schuch, I. Cirac, and D. Pérez-García, Peps as ground states: Degeneracy and topology, *Ann. Phys. (Amsterdam)* **325**, 2153 (2010).
- [70] A. Molnar, A. Ruiz de Alarcón, J. Garre-Rubio, N. Schuch, J. I. Cirac, and D. Pérez-García, Matrix product operator algebras I: Representations of weak Hopf algebras and projected entangled pair states, [arXiv:2204.05940](https://arxiv.org/abs/2204.05940).
- [71] A. Ruiz-de-Alarcon, J. Garre-Rubio, A. Molnar, and D. Perez-Garcia, Matrix product operator algebras II: Phases of matter for 1D mixed states, [arXiv:2204.06295](https://arxiv.org/abs/2204.06295).
- [72] E. Zohar, M. Burrello, T. B. Wahl, and J. I. Cirac, Fermionic projected entangled pair states and local $U(1)$ gauge theories, *Ann. Phys. (N.Y.)* **363**, 385 (2015).
- [73] P. Emonts and E. Zohar, Gauss law, minimal coupling and fermionic PEPS for lattice gauge theories, *SciPost Phys. Lect. Notes* **12** (2020). [10.21468/SciPostPhysLectNotes.12](https://arxiv.org/abs/10.21468/SciPostPhysLectNotes.12)
- [74] P. Emonts and E. Zohar, Fermionic Gaussian PEPS in $3 + 1d$: Rotations and relativistic limits, *Phys. Rev. D* **108**, 014514 (2023).
- [75] Y.-H. Wu, L. Wang, and H.-H. Tu, Tensor network representations of parton wave functions, *Phys. Rev. Lett.* **124**, 246401 (2020).
- [76] H.-K. Jin, H.-H. Tu, and Y. Zhou, Efficient tensor network representation for Gutzwiller projected states of paired fermions, *Phys. Rev. B* **101**, 165135 (2020).
- [77] G. Petrica, B.-X. Zheng, G. K.-L. Chan, and B. K. Clark, Finite and infinite matrix product states for Gutzwiller projected mean-field wave functions, *Phys. Rev. B* **103**, 125161 (2021).
- [78] H.-K. Jin, H.-H. Tu, and Y. Zhou, Density matrix renormalization group boosted by Gutzwiller projected wave functions, *Phys. Rev. B* **104**, L020409 (2021).
- [79] J.-W. Li, J. von Delft, and H.-H. Tu, $U(1)$ -symmetric Gaussian fermionic projected entangled paired states and their Gutzwiller projection, *Phys. Rev. B* **107**, 085148 (2023).
- [80] Q. Yang, X.-Y. Zhang, H.-J. Liao, H.-H. Tu, and L. Wang, Projected d-wave superconducting state: A fermionic projected entangled pair state study, *Phys. Rev. B* **107**, 125128 (2023).
- [81] H.-K. Jin, R.-Y. Sun, Y. Zhou, and H.-H. Tu, Matrix product states for Hartree-Fock-Bogoliubov wave functions, *Phys. Rev. B* **105**, L081101 (2022).
- [82] M. T. Fishman and S. R. White, Compression of correlation matrices and an efficient method for forming matrix product states of fermionic Gaussian states, *Phys. Rev. B* **92**, 075132 (2015).
- [83] C. Wille, O. Buerschaper, and J. Eisert, Fermionic topological quantum states as tensor networks, *Phys. Rev. B* **95**, 245127 (2017).
- [84] A. Hackenbroich, B. A. Bernevig, N. Schuch, and N. Regnault, Fermionic tensor networks for higher-order topological insulators from charge pumping, *Phys. Rev. B* **101**, 115134 (2020).
- [85] S. K. Shukla, T. D. Ellison, and L. Fidkowski, Tensor network approach to two-dimensional bosonization, *Phys. Rev. B* **101**, 155105 (2020).
- [86] L. Wang, P. Corboz, and M. Troyer, Fermionic quantum critical point of spinless fermions on a honeycomb lattice, *New J. Phys.* **16**, 103008 (2014).
- [87] B.-X. Zheng, C.-M. Chung, P. Corboz, G. Ehlers, M.-P. Qin, R. M. Noack, H. Shi, S. R. White, S. Zhang, and G. K.-L. Chan, Stripe order in the underdoped region of the two-dimensional Hubbard model, *Science* **358**, 1155 (2017).
- [88] Z. Dai, Y. Wu, T. Wang, and M. P. Zaletel, Fermionic isometric tensor network states in two dimensions, [arXiv:2211.00043](https://arxiv.org/abs/2211.00043).
- [89] Y. Ma, S. Jiang, and C. Xu, Variational tensor wavefunctions for the interacting quantum spin Hall phase, [arXiv:2302.03879](https://arxiv.org/abs/2302.03879).
- [90] C. Xu, Y. Ma, and S. Jiang, Unveiling correlated topological insulators through fermionic tensor network states—classification, edge theories and variational wavefunctions, [arXiv:2308.06543](https://arxiv.org/abs/2308.06543).